ON THE WAY TO RELIABLE AEROELASTIC LOAD SIMULATION ON VAWT'S.

PRESENTED AT EWEA 2013 CONFERENCE, VIENNA

Torben J. Larsen
DTU Wind Energy
DK-4000 Roskilde
Denmark
Email: tjul@dtu.dk

Helge Aagaard Madsen
DTU Wind Energy
DK-4000 Roskilde
Denmark
Email: hama@dtu.dk

ABSTRACT

In this paper a method for an implementation of a 2D actuator cylinder flow model of an Vertical Axis Wind Turbine (VAWT) is presented. The model is implemented in a full aeroelastic code including consideration of structural dynamics, dynamic inflow, tower shadow and dynamic stall, which is needed for a full load analysis relating to eg. certification of a VAWT turbine. Further on, principal load cases according to the IEC61400-1 are simulated for a fictitious 5MW VAWT turbine in it's simplest 2 bladed Darrieus configuration. The IEC61400-1 load cases, originally developed for Horizontal Axis Wind Turbines (HAWT's), are discussed regarding the application to VAWT's. Further on a small section regarding aerodynamic flow in curved motion is included.

1 INTRODUCTION

Within the last few years VAWT's have gained renewed interest as a potential competitive wind turbine design and not least for off-shore applications. This is mainly due to the basically simple concept with main features such as 1) no yaw system; 2) stall controlled and therefore no pitch system and a low centre of gravity which could be an advantage for floating turbine concepts. However, the design and dimensioning of VAWT's requires that a detailed aeroelastic analysis can be performed. Also for the certification, a comprehensive load basis comprising fatigue as well as ultimate loads is required. Although many parts from the aeroelastic analysis and certification of HAWT's, developed over at least 25 years, there are also some fundamental differences which requires a different aeroelastic modeling and possibly also some differences in load cases for certification. The VAWT differs fundamentally from a HAWT in the way that the swept surface of a VAWT is fully three-dimensional extending in three directions along the main wind direction and in the horizontal and vertical direction, whereas the swept area of a HAWT has no significant extension in the streamwise direction. With atmospheric turbulent inflow to the rotor this leads to basic differences in load characteristics. For a MW VAWT with a maximum rotor radius of e.g. 60-80m it means that a gust passing the front part of the rotor will pass the rear part with a delay of several seconds depending on the mean wind speed. The influence on the overall rotor thrust is expected to be a stronger filtering of turbulence that for a HAWT of the same size. Also some of the extreme load cases defined for VAWTt's will have a different impact on a VAWT and probably needs more specification. The so called Mexican hat (extreme operating gust) variation of the wind speed is one example which will have less influence on the thrust force variation of a VAWT due to the extension of the swept area in the streamwise direction. The aeroelastic analysis requires that the aeroelastic code is designed to model the basic aerodynamics of the VAWT and not only for uniform, steady inflow as has mainly been considered so far, but also for atmospheric turbulent inflow which is necessary for design and certification of a VAWT for big scale application. The present paper describes the adaptation of the HAWC2 code for aeroelastic VAWT simulations. This comprises the incorporation of the Actuator Cylinder flow model [1], [2] regarding modeling of aerodynamic induction which will be briefly described in the paper. Next several different load cases will be presented and the fundamental differences in aeroelastic response compared with HAWT's will be discussed.

2 INDUCTION MODELING OF VAWT's IN HAWC2

The aerodynamic problem for vertical axis wind turbines is quite complex and different of a horizontal axis wind turbine. This is traditionally handled using double stream turbe momentum modeling or using more complex aerodynamic methods like vortex and CFD simulation, whereas the latter are very computationally demanding. In this paper it is suggested to reduce the flow problem by condensing the three dimensional case to a number of 2D cylinders stacked vertically. For the 2D case it is possible to find the steady state solution in a fairly easy way using a modified linear solution of the actuator cylinder approach. The benefits of this is a more physical correct solution than the double stream tube method and a very computational efficient and fast approach compared to vortex and full CFD solutions. A drawback compared to the latter mentioned methods are the neglection of the discrete vortices from the upwind blades circulation transported downstream, affecting the downstream blades. The impact of this is expected to be of minor importance compared to the ambient turbulent inflow, which however need validation.

2.1 Finding the 2D loads in the right coordinate system

First step is to define the relevant coordinate systems used in the analysis, as illustrated in Figure 1. The initial coordinate system is $\{x,y,z\}_G^T$, where the z is vertical downward and y is in the default horizontal wind direction. The VAWT's shaft rotation vector is denoted ω. For every calculation point along the blade a cross section forming a disc perpendicular to ω is created. Such a cross section is shown in Figure 1 using the index A-A. The disc coordinate system $\{x,y,z\}_D^T$ is created, where the transformation matrix from disc to global coordinates is denoted $\mathbf{T}_{DG}$. In order to enable a 2D solution of the flow problem in the disc plane, the $\{x,y,z\}_D^T$ is created so the z-direction is along ω. In this plane, the x and y is oriented so x is along the direction of the average wind speed. One method of doing this could be to first generate a temporary coordinate system $\mathbf{T}'_{DG}$ with the z along ω and x and y defined orthogonal but otherwise randomly. The free wind speed vector V_∞ (obtained as an average vector over the disc based on the previous time step) is projected to the disc

$$V'_\infty = \mathbf{T}'_{DG} V_\infty \tag{1}$$

and the angle γ between the wind speed V'_∞ and the x_D coordinate is now found

$$\gamma = \arctan\left(\frac{V'_\infty(2)}{V'_\infty(1)}\right) \tag{2}$$

The final orientation of the disc coordination can then be found by eg. a vector rotation of x,y around z in $\mathbf{T}'_{DG}$ by the angle γ using a method inspired by Rodrigues formula. In (3) the vector $\mathbf{x}$ is the vector to be rotated around $\mathbf{n}$ with the angle γ. $\mathbf{x}$ and $\mathbf{n}$ are formulated in global coordinates.

$$\mathbf{x}_{new} = \mathbf{n}(\mathbf{n}\cdot\mathbf{x} + \cos\gamma(\mathbf{x} - \mathbf{n}(\mathbf{n}\cdot\mathbf{x}))) + \sin\gamma(\mathbf{n}\times\mathbf{x}) \tag{3}$$

or more simply using an extra transformation matrix.

$$\mathbf{T}_{DG} = \begin{bmatrix} \cos\gamma & \sin\gamma & 0 \\ -\sin\gamma & \cos\gamma & 0 \\ 0 & 0 & 1 \end{bmatrix} \mathbf{T}'_{DG} \tag{4}$$

When the $\mathbf{T}_{DG}$ is found, the polar coordinate system x,y,z_P can be obtained for every calculation point in the grid based on a rotation with the azimuth angle φ.

$$\mathbf{T}_{PG,i} = \begin{bmatrix} \cos\varphi_i & \sin\varphi_i & 0 \\ -\sin\varphi_i & \cos\varphi_i & 0 \\ 0 & 0 & 1 \end{bmatrix} \mathbf{T}_{DG} \tag{5}$$

In this 2D plane, aerodynamic forces are calculated based on 2D look-up tables giving the relationship between C_l, C_d and the angle of attack α as shown in Figure 3. However, since we later need to have the aeroynamic forces in all points around the circle, we need to find the forces in these points as if the blade was in that position. This basically follows an assumption of infinitive number of blades well known from classic BEM theory.

In each point the local inflow velocity in local coordinates ($\mathbf{V}_L$) is found based on a relationship between the free inflow velocity ($\mathbf{V}_{\mathrm{inf},G}$), the local induced wind speed ($\mathbf{V}_{induc,G}$) and the profiles own velocity ($\mathbf{V}_{L,G}$). All vectors used, are related to the local point in focus and transformed from global coordinates (index G) to local section coordinates (index L). The local L coordinate system being defined with the x_L axis through the chord line and z_L through the centerline of the blade, see Figure 2.

$$\mathbf{V}_L = \mathbf{T}_{GL}(\mathbf{V}_{\mathrm{inf},G} + \mathbf{V}_{induc,G} - \mathbf{V}_{L,G}) \tag{6}$$

In each point the free wind speed is found by a lookup in the turbulence box, whereas the induced wind speed is based upon an already calculated induced velocity in a previous time step or iteration. It is more difficult to find the profiles own velocity as the profiles is not necessarily located at this position. What we do know is the velocity of the blade profile

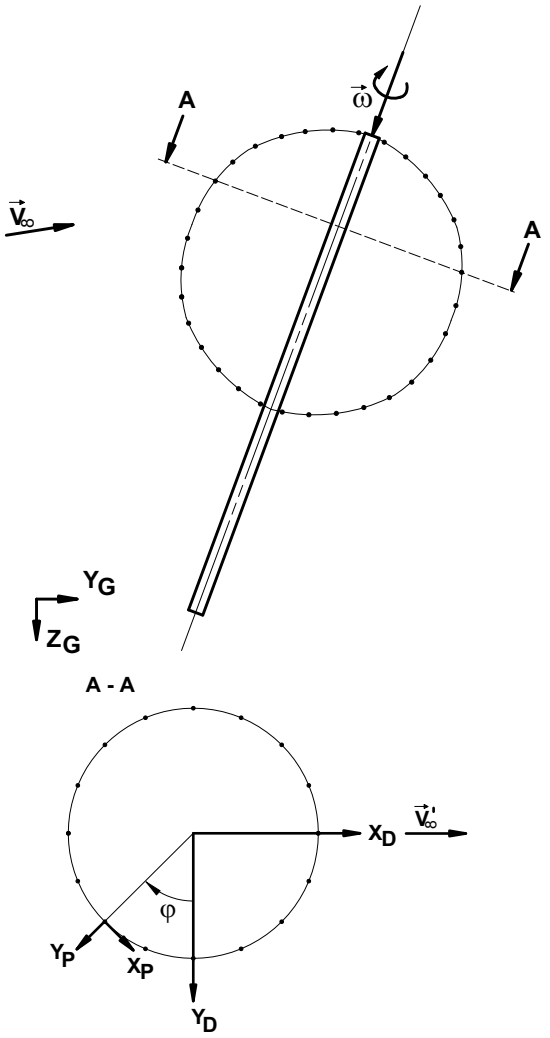

FIGURE 1: The vawt is subdivided into a number of 2D discs, each with calculation points around the full circumference is defined. Notations used for the coordinate transformations are also shown.

at its present location $\mathbf{V}_{S,G}$. Using a simple transformation around the VAWT's rotation axis ω we get an estimate of the profile velocity if it had been at this location.

This is done using the Rodrigues method (3), where $\mathbf{V}_{S,G}$ is rotated around ω with the angle $\varphi_L - \varphi_S$.

The transformation matrix $\mathbf{T}_{GL}$ is created based on the orientation matrix for the profile $\mathbf{T}_{SG}$, where each matrix column (representing the local coordinate vectors) is rotated using Rodrigues in similar way as for the $\mathbf{V}_{S,G}$ vector. The angle

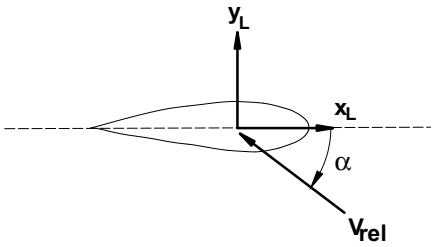

FIGURE 2: Illustration showing the L coordinate system.

of attack and the relative velocity V_r is now found

$$\alpha = \arctan\left(\frac{\mathbf{V}_L(1)}{\mathbf{V}_L(2)}\right) \tag{7}$$

$$V_r = \sqrt{\mathbf{V}_L(1)^2 + \mathbf{V}_L(2)^2} \tag{8}$$

The lift L and drag D is found and transformed to radial and tangential coordinates. This is done by a simple transformation of the lift and drag coefficients to polar coordinates, where the coefficients is assembled to a vector $\mathbf{C}_P$.

$$\mathbf{C}_P = \mathbf{T}_{GP}\mathbf{T}_{LG}\begin{bmatrix} -\cos\alpha & \sin\alpha & 0 \\ -\sin\alpha & \cos\alpha & 0 \\ 0 & 0 & 1 \end{bmatrix}\begin{Bmatrix} C_d \\ C_l \\ 0 \end{Bmatrix} \tag{9}$$

In each point the radial and tangential loadings F_r and F_t are found.

$$F_r = \frac{1}{2}\rho c V_r^2 \mathbf{C}_P(2) \tag{10}$$

$$F_t = \frac{1}{2}\rho c V_r^2 \mathbf{C}_P(1) \tag{11}$$

which is used to determine the non-dimensional loading from the VAWT on to the flow in radial and tangential direction Q_r and Q_t.

$$Q_r = \frac{NF_r}{2\pi R\rho V_\infty^2} \tag{12}$$

$$Q_t = \frac{NF_t}{2\pi R\rho V_\infty^2} \tag{13}$$

which leads to

$$Q_r = \frac{-V_r^2 \mathbf{C}_P(2) cN}{4\pi R V_\infty^2} \tag{14}$$

$$Q_t = \frac{V_r^2 \mathbf{C}_P(1) cN}{4\pi R V_\infty^2} \tag{15}$$

Later in the paper, the average thrust coefficient is needed for the 2D flow solution. This thrust coefficient is defined

$$C_T = \frac{T}{\frac{1}{2}\rho A V_\infty^2} \tag{16}$$

where the area per length unit A corresponds to $2R$

In it simplest case, where the VAWT's blades are parallel to the rotation vector ω, C_T is found

$$C_T = \frac{\frac{1}{2\pi R}\int_0^{2\pi}(F_n(\varphi)\sin\varphi - F_t(\varphi)\cos\varphi)NRd\varphi}{\frac{1}{2}\rho A V_\infty^2} \tag{17}$$

which can be condensed to

$$C_T = \int_0^{2\pi}(Q_r(\varphi)\sin\varphi - Q_t(\varphi)\cos\varphi)d\varphi \tag{18}$$

However, the blades are in most case not perpendicular to the rotation axis ω and a more general expression than (18) is written in (19).

$$C_T = \int_0^{2\pi} \mathbf{T}_{GR}\mathbf{T}_{PG}\{-Q_t, -Q_r, 0\}^T d\varphi \tag{19}$$

2.2 Solution of the 2D quasistatic flow problem

The solution of the 2D flow problem shown in section A-A in Figure 1 is obtained using a method described in [2]. This solution is based on a modified linear solution of a so-called actuator cylinder model, originally described in [1]. The forces on a cylinder is inserted as shown in Figure 4.

The local velocities w_x and w_y representing the changes in wind speed due to the presence of the VAWT are defined

$$v_x = 1 + w_x \tag{20}$$

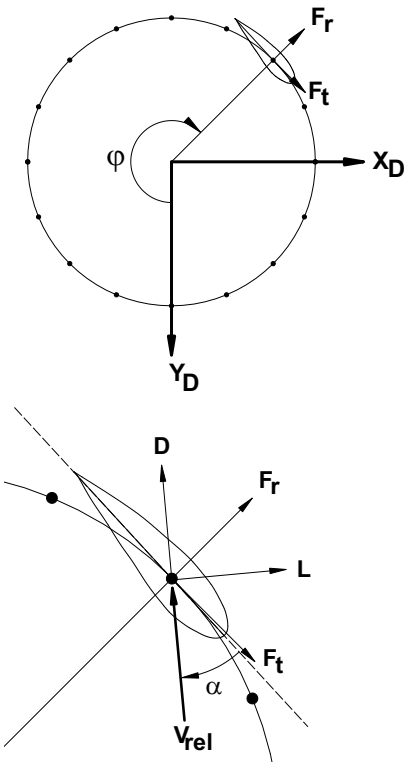

FIGURE 3: Local blade profile and corresponding notation used in 2D blade analysis. Top: overview of radial and tangential forces on the airfoil section. Bottom: Zoom of airfoil sections with local aerodynamic properties in a BEM analysis, including relative velocity V_{rel} angle of attack α, Lift L and Drag D forces.

$$v_y = w_y \tag{21}$$

In 20 and 21 and in the following, all velocities are non-dimensioned with the free velocity $V_{\infty,disc}$ and distances with rotor radius R

2.2.1 Linear solution

The linear solution of the actuator cylinder problem to the actuator cylinder models was in [1] and later written in [2] found to be

$$w_x = -\frac{1}{2\pi}\int_0^{2\pi} Q_r(\varphi)\frac{-(x+\sin\varphi)\sin\varphi + (y-\cos\varphi)\cos\varphi}{(x+\sin\varphi)^2 + (y-\cos\varphi)^2}d\varphi$$
$$-Q_r(\arccos(y))^* + Q_r(-\arccos(y))^{**} \tag{22}$$

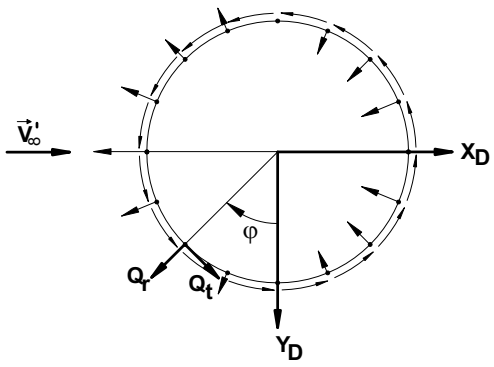

FIGURE 4: The actuator cylinder flow model with radial and tangential loading. Note the force direction is from the VAWT onto the flow resulting in opposite sign than F_t and F_r. Arrows show typical force direction on the flow, however Q_r is defined positive outwards always.

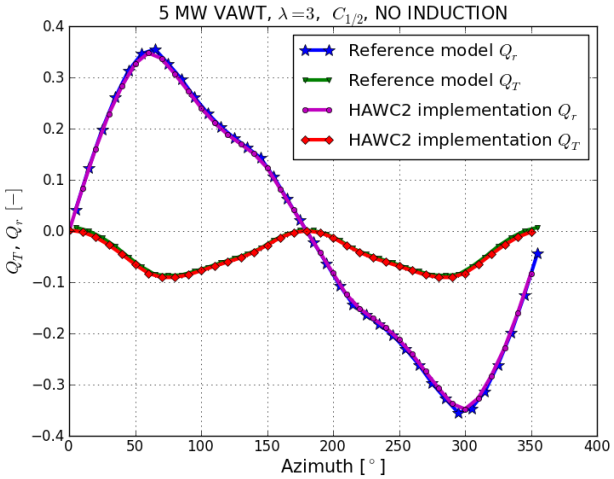

FIGURE 5: Comparison of loading on the rotor without influence of induced velocities between the reference model used in [2] and the present implementation in HAWC2.

$$w_y = -\frac{1}{2\pi}\int_0^{2\pi} Q_r(\theta)\frac{-(x+\sin\varphi)\cos\varphi-(y-\cos\varphi)\sin\varphi}{(x+\sin\varphi)^2+(y-\cos\varphi)^2}d\varphi \tag{23}$$

This solution represents the modified flow both out- and inside the VAWT, obtained through the coordinates x and y (non-dimensioned position with the VAWT disc radius). The term marked with * in equation (22) shall only be added inside the cylinder whereas in the wake behind the cylinder, both the term marked with * and ** shall be added.

Assuming that the loading is piece wise linear, the equations (22) and (23) can be rewritten in discrete form

$$w_x = -\frac{1}{2\pi}\sum_{i=1}^{i=N} Q_{r,i}\int_{\varphi_i-\frac{1}{2}\Delta\varphi}^{\varphi_i+\frac{1}{2}\Delta\varphi}\frac{-(x+\sin\varphi)\cos\varphi-(y-\cos\varphi)\sin\varphi}{(x+\sin\varphi)^2+(y-\cos\varphi)^2}d\varphi \tag{24}$$

$$w_y = -\frac{1}{2\pi}\sum_{i=1}^{i=N} Q_{r,i}\int_{\varphi_i-\frac{1}{2}\Delta\varphi}^{\varphi_i+\frac{1}{2}\Delta\varphi}\frac{-(x+\sin\varphi)\cos\varphi-(y-\cos\varphi)\sin\varphi}{(x+\sin\varphi)^2+(y-\cos\varphi)^2}d\varphi \tag{25}$$

where the index i (and later also j) represents the calculation point number starting with 1 for $\varphi = 0°$.

Since the coordinate system of the disc is always aligned with the incoming wind direction and we only are interested in velocities at the disc circumference, the integration expression in (24) and (25) remain constant with time and can therefore be calculated initially prior to the actual time simulation.

$$w_{x,j} = -\frac{1}{2\pi}\sum_{i=1}^{i=N} Q_{r,i}R_{wx,i,j} - Q^*_{r,j} + Q^*_{r,(N-j)} \tag{26}$$

$$w_{y,j} = -\frac{1}{2\pi}\sum_{i=1}^{i=N} Q_{r,i}R_{wy,i,j} \tag{27}$$

with the influence coefficients R_{wx} R_{wy} in point j influenced by all the other points $i = 1..N$. These values are initially calculated once and for all.

$$R_{wx,j,i} = \int_{\varphi_i-\frac{1}{2}\Delta\varphi}^{\varphi_i+\frac{1}{2}\Delta\varphi}\frac{-(x+\sin\varphi)\cos\varphi-(y-\cos\varphi)\sin\varphi}{(x+\sin\varphi)^2+(y-\cos\varphi)^2}d\varphi \tag{28}$$

$$R_{wy,j,i} = \int_{\varphi_i-\frac{1}{2}\Delta\varphi}^{\varphi_i+\frac{1}{2}\Delta\varphi}\frac{-(x+\sin\varphi)\cos\varphi-(y-\cos\varphi)\sin\varphi}{(x+\sin\varphi)^2+(y-\cos\varphi)^2}d\varphi \tag{29}$$

2.2.2 Modified linear solution

The linear solution is in general in good agreement with the full actuator cylinder model, however especially on the downwind side of the rotor, deviations can be seen, see Figure 6.

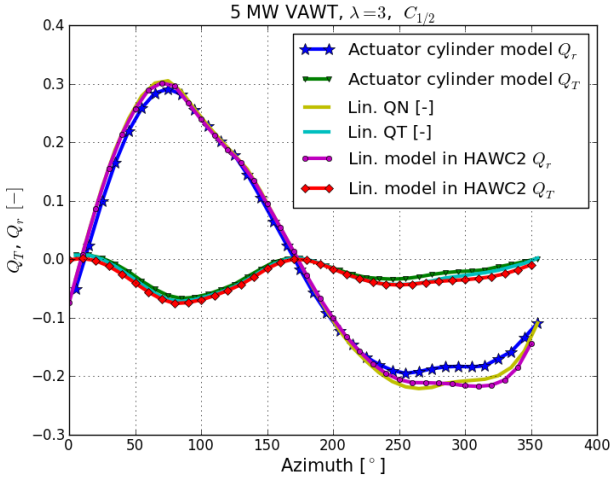

FIGURE 6: Comparison of loading on the rotor including induced velocities predicted through the linear solution.

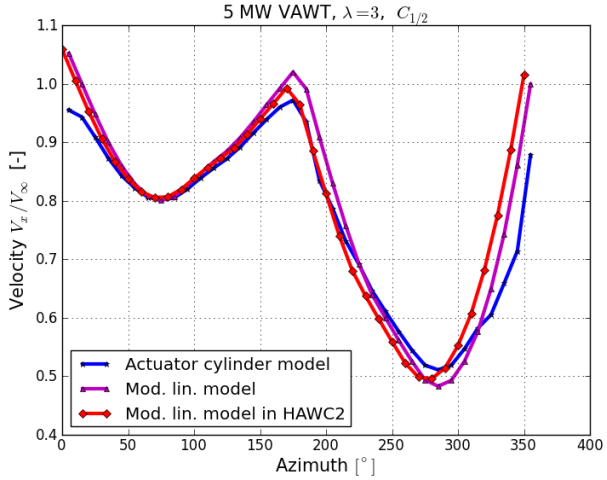

FIGURE 7: Comparison of axial velocity as function of azimuth angle.

This was addresses by Madsen [2] and a very simple correction term was added resulting in a remarkable improvement of the linear solution. The basis for the correction term is that a uniformly loaded VAWT with the linear solution obtains the following relation between thrust coefficient C_T and the induction a.

$$C_T = 4a_{linear} \tag{30}$$

However from the classic BEM theory for horizontal axis wind turbines (HAWT), the relation is

$$C_T = 4a(1-a) \tag{31}$$

A simple correction function (32) is suggested to be multiplied on the terms w_x and w_y found using the linear solution, which makes the final solution in better agreement with both the nonlinear VAWT solution as well as the solution approach of a HAWT.

$$k_a = \frac{1}{1-a} \tag{32}$$

The induction a used in (32) is found for the disc based on the average thrust coeffient C_T as found in (19) through a polynomial relationship between C_T and a as used in the practical BEM implementation used for HAWT's in HAWC2 [**?**]. This polynomium includes the $C_T = 4a(1-a)$ as well as the Glauert correction for a>0.5.

$$a = k_3 C_T^3 + k_2 C_T^2 + k_1 C_T + k_0 \tag{33}$$

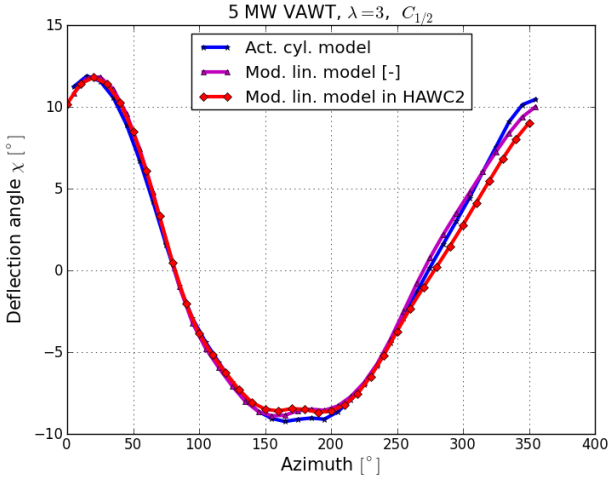

FIGURE 8: Comparison of horizontal flow deflection angle.

with $k_3 = 0.0892074$, $k_2 = 0.0544955$, $k_1 = 0.251163$ and $K_0 = -0.0017077$.

2.3 Time filtering of the induced velocities

As for a HAWT, it is clear that induced velocities cannot get to a steady state equilibrium without time for this to happen. The mass flow through the rotor is substantial and a change in rotor loading will first cause a different balance between thrust and induced velocities after a while.

We propose this to be modeled in similar way as for a HAWT, where the dynamic inflow is normally modeled using

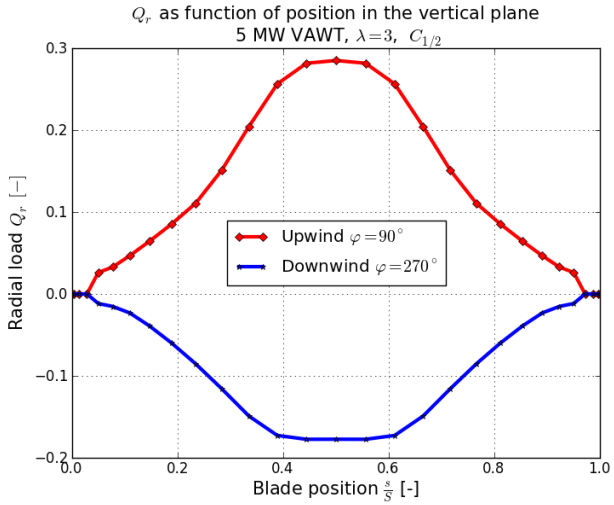

FIGURE 9: Radial load extracted as function of position on the blade at azimuth 90 and 270° using the modified linear model implemented in HAWC2.

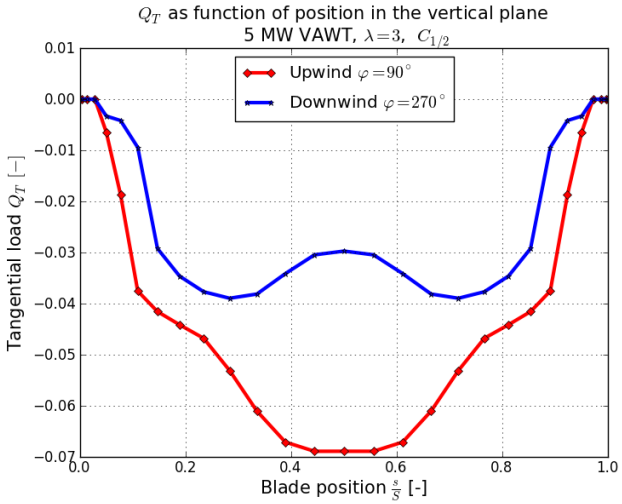

FIGURE 10: Radial load extracted as function of position on the blade at azimuth 90 and 270° using the modified linear model implemented in HAWC2.

a low pass filtering of the calculated steady state induced velocities. In the HAWC2 code, this is being done for HAWT's with great success using two first order filter coupled in parallel with weight functions as originally described in [3]. The idea of using two first order filter functions is that one filter represents the near wake effects with a non-dimensional time constant τ^* of approximately 0.5 and another filter represents the far wake with a non-dimensional time constant of 2.0. Both time constants being non-dimensional with rotor Radius and the average wake velocity $\tau = \tau^* \frac{R}{V_{wake}}$. Since we so far does not know any better, we propose a similar approach for a VAWT and similar time constants too. The weight of the near wake filter is 0.6 and 0.4 for the far wake filter.

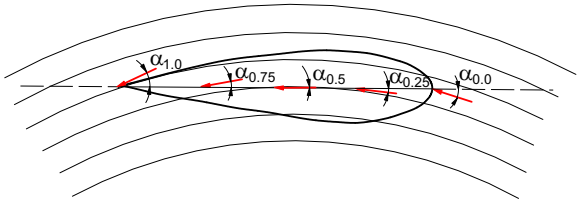

FIGURE 11: Difference in angle of attack at an airfoil section in curved motion.

A first order filter with the time constant τ is in LaPlace domain formulated. The raw signal is here denoted q, where the filtered signal is noted y

$$y = \frac{1}{1+s\tau} q \tag{34}$$

which can be formulated in discrete time domain using eg. an indicial function formulation. The index $(_1)$ refers to one time step earlier, assuming a constant discrete time step ΔT

$$y = y_1 \exp\left(-\frac{\Delta T}{\tau}\right) + q\left(1 - \exp\left(-\frac{\Delta T}{\tau}\right)\right) \tag{35}$$

3 A comment on airfoil sections in curved motion

An interesting effect of airfoil sections in a VAWT configuration is that the individual blade sections experience a curved inflow due to it's own rotation velocity. For a very slender blade on a large radius, the angle of attack is more or less the same over the entire chord, but for a more realistic solidity, the angle of attack varies over the chord length. This was treated by de Vries [4] where it was concluded that the appropriate angle of attack is the average between $\alpha_{0.5}$ and $\alpha_{1.0}$. In HAWC2 it was chosen to use $\alpha_{0.75}$ directly as this was in line with the approach already used for dynamic inflow of a horizontal axis wind turbine. This is also the requirement for using the build in dynamic stall model [5], [6].

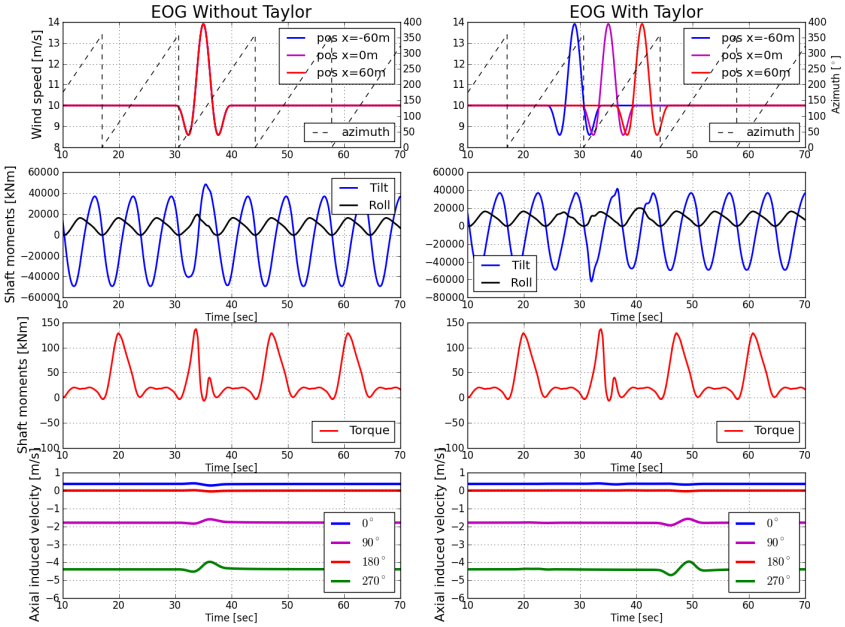

FIGURE 12: An example of the difference in response to an extreme operating gust with and without consideration of Taylor's hypothesis.

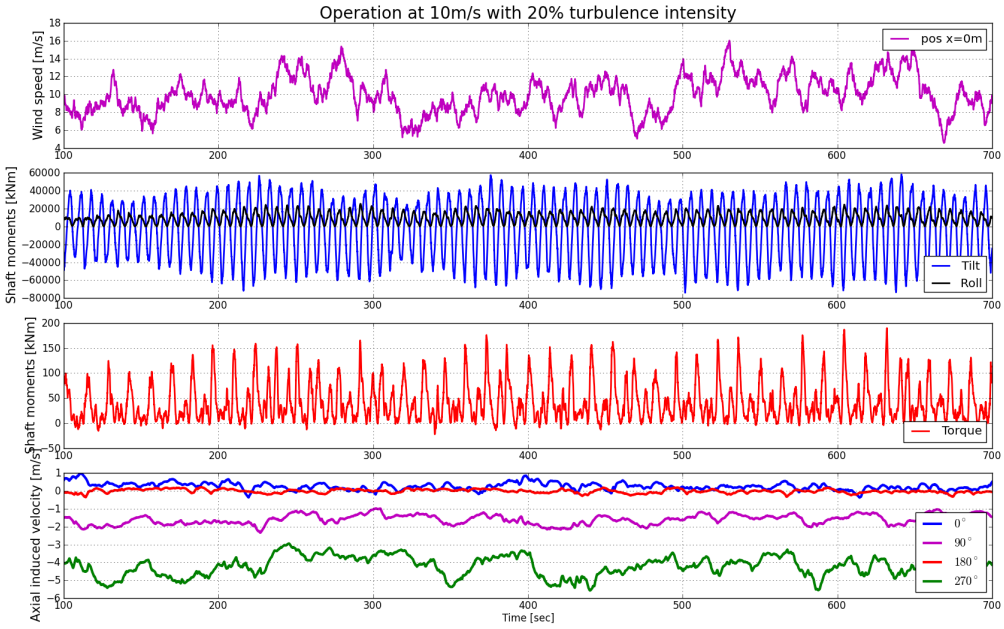

FIGURE 13: Loads during normal operation at 10m/s with 20% turbulence intensity.

4 IEC load cases

Dealing with turbulent and other transient gust flow situations the usage of Taylors hypothesis [7] may be more important for VAWT's than HAWT's due to the three-dimensional rotor extension. In this chapter especially the extreme operating gust (EOG) is investigated with the present IEC formulation as well as in slightly modified form where Taylors hypothesis is used, see (36). In this hypothesis it is assumed that the mean wind speed is much higher that the turbulent velocity and it can reasonable be assumed the turbulent eddies are constant and transported with the mean wind speed. The main effect is that there is a direct relation between time and position of the large scales in turbulent inflow. If the extreme operating gust represents a frontal passage it also seem appropriate that Taylor's relation is applied. The response is investigated for a rigid VAWT operating at 10m/s during an EOG with a gust size V_{gust} of 5.28m (class IA conditions), see Figure 12. Even though the impact of the EOG is not particularly pronounced compared to the large load variation from the normal aerodynamic loads, it can still be seen that the response is different when Taylor's hypothesis is included.

$$x \simeq Ut \tag{36}$$

$$V(z,t) = V(z) - 0.37V_{gust}\sin(3\pi t/T)(1-\cos(2\pi t/T)) \tag{37}$$

$$V(z,x,t) = V(z) - 0.37V_{gust}\sin(\frac{3\pi(t-x/U)}{T})(1-\cos(\frac{2\pi(t-x/U)}{T})) \tag{38}$$

The response of the turbine in turbulent inflow is shown in Figure 13. The mean wind speed is 10m/s and the turbulence intensity is 20%. Even though the load is still highly deterministic due to the configuration of the VAWT with two vertical blades (in contrast to a perhaps better configuration with e.g. three helical shaped blades) the impact of turbulence is highly noticeable. The non-constant induced velocity at four selected azimuthal locations is also shown.

5 Conclusions

In this paper a new approach to simulate the complex flow of a VAWT has been presented with special attention to the implementation of a 2D actuator cylinder model in a full 3D multibody aeroelastic code for load simulation in time domain. The model has been extended from a quasi steady approach with a dynamic inflow model approach known from dynamic BEM formulations of HAWT simulations. Improvement of this model approach is still yet to be done, especially regarding finding the right time constants, however initial results of full loading of a Darrieus VAWT is presented in both fully turbulent as well as gust load cases. In the present formulation of the IEC61400-1 standard, the gust load cases are specified as function of time and height only. In this paper, it is suggested to extend these gust case formulations between time and space using Taylor's hypothesis and the influence of this more physical correct approach is demonstrated for an extreme operating gust.

REFERENCES

[1] Madsen, H. A., 1982, "The Actuator Cylinder, a flow model for vertical axis wind turbines. PhD thesis, Part 1,2 and 3," Tech. rep., Aalborg university centre.

[2] Madsen, H., T.J., L., Vita, L., and Paulsen, U., 2013, "Implementation of the Actuator Cylinder flow model in HAWC2 for aeroelastic simulations on Vertical Axis Wind Turbines," *Proceedings of the 51st AIAA Aerospace Sciences Meeting, Dallas*, AIAA.

[3] Sørensen, N. and Madsen, H. A., 2006, "Modelling of transient wind turbine loads during pitch motion," *Online proceedings. European Wind Energy Conference and Exhibition, Greece, 27 Feb - 2 March 2006*, EWEA.

[4] DeVries, O., 1979, "Fluid dynamic aspects of wind energy conversion," Tech. Rep. AGARD-AG-243, ISBN-92-835-1326-6, NATO Science and Technology Organization.

[5] Leishman, J. and Beddoes, T., 1986, "A generalized model for airfoil unsteady aerodynamic behaviour and dynamic stall using the indicial method," *Proceeding of the 42end Annual Forum of the American Helicopter Society*.

[6] Hansen, M. H., Gaunaa, M., and Madsen, H., 2004, "A Beddoes-Leishman type dynamic stall model in state-space and indicial formulations," Tech. Rep. Risø-R-1354(EN), Risoe National Laboratory.

[7] Taylor, G., 1937, "The spectrum of turbulence," Proc. R. Soc. Lond. A, **164**, pp. 476–490.

ACKNOWLEDGMENT

The work has been funded by the european FP7 programme within the project *DeepWind*. Acknowledgement for European Commission, Grant 256769 FP7 Energy 2010- Future emerging technologies, and by the DeepWind beneficiaries: DTU(DK), AAU(DK), TUDELFT(NL), TUTRENTO(I), DHI(DK), SINTEF(N), MARINTEK(N), MARIN(NL), NREL(USA), STATOIL(N), VESTAS(DK) and NENUPHAR(F).